The Role of Self-Focusing During the Laser Microstructuring in the Volume of Fused Silica

Anna V. Bogatskaya[1,2][a], Ekaterina A. Volkova[3][b] and Alexander M. Popov[1,2][c]

[1]Department of Physics, Lomonosov Moscow State University, 119991, Moscow, Russia
[2]Lebedev Physical Institute, Russian Academy of Sciences, 119991, Moscow, Russia
[3]Skobeltsyn Institute of Nuclear Physics, Lomonosov Moscow State University, 119991, Moscow, Russia

Keywords: Laser Microstructuring in Dielectrics, Birefringent Nanolattices, Fused Silica, Multiphoton Ionization of Dielectrics, Plasma Formation, Numerical Modelling, Wave Equation.

Abstract: In this study we perform 3D self-consistent numerical simulations of a focused laser pulse exposure in the bulk of fused silica. The model combines the second-order wave equation in cylindrical coordinates with a rate equation for the density of charge carriers in the conduction band. Our results indicate that a dense plasma formation near the focal plane effectively scatters and reflects the laser pulse. The coherent interference between the incident and scattered laser waves creates regions of intense field ionization, resulting in periodic plasma nanostructures along both the ρ- and z-axes. We also examine the impact of nonlinear refractive index effects, which lead to pulse self-focusing. We should note that similar subwavelength, divergent structures in material modification regions have been observed in recent experiments conducted under comparable laser focusing conditions.

1 INTRODUCTION

In recent years, substantial research has been dedicated to investigating the complex, multi-level processes that modify the physical characteristics of materials subjected to tightly focused femtosecond laser pulses (Gattass and Mazur, 2008; Taylor et al., 2007; Bulgakova et al., 2015). State-of-the-art ultrafast laser systems have revealed new mechanisms in how electromagnetic fields, plasma, and materials interact. These interactions drive various structural changes in transparent dielectric materials, such as the formation of micro- and nanoscale voids, densification zones, micro-tracks (Shimotsuma et al., 2005; Sun et al., 2007; Beresna et al., 2011; Dai et al., 2016; Mizeikis et al., 2009), as well as periodic refractive index shifts (Schaffer et al., 2001; Wang et al., 2007; Mermillod-Blondin et al., 2008) and other effects.

One of the most notable achievements has been the development of periodic subwavelength structures with high optical contrast between modified zones, which are particularly promising for applications in optical memory, micro-photonic crystals, optical couplers, binary storage, and other fields (Musgraves et al., 2011; Tan et al., 2016). Among these materials, fused silica glass has become especially important since the groundbreaking work of (Shimotsuma et al. 2003), which first introduced the concept of birefringent volume nanogratings in this medium. Subsequent research by various groups (Desmarchelier et al., 2015; Bulgakova et al., 2013) has highlighted key mechanisms involved in creating these structures. These mechanisms include coupling between electron plasma waves and incident light (Shimotsuma et al., 2005; Shimotsuma et al., 2003), the formation of nanoplasmas due to field localization and their self-organization into nanoscale patterns (Bhardwaj et al., 2006; Taylor et al., 2008), and the confinement and clustering of exciton-polaritons (Beresna et al., 2012). However, the lack of comprehensive theoretical models to confirm each proposed mechanism, as well as an incomplete understanding of the necessary conditions, still

[a] https://orcid.org/0000-0002-1538-3433
[b] https://orcid.org/0000-0002-4883-3349
[c] https://orcid.org/0000-0002-7300-3785

presents challenges to the controlled and precise laser fabrication of these complex volume nanopatterns.

In this work, we carry out fully self-consistent 3D numerical simulations of the propagation of an intense, tightly focused Yb-doped fiber laser pulse ($\lambda_0 = 1030$ nm) in fused silica, alongside the dynamics of laser-induced solid-state plasma. The simulations explore a range of pulse durations, peak intensities, and focusing parameters. By including the curvature of the incident laser pulse front and considering scattering and diffraction effects in cylindrical geometry, we identified a new mechanism of plasma self-organization in conditions of tight laser beam focusing. The findings reveal that dense plasma formation near the focal area effectively scatters the laser wave. Due to the interference between the incident plane wave and the reflected, highly non-planar wave in the pre-focal area, a detailed pattern of laser field amplitude peaks and troughs emerges, leading to a structured subwavelength plasma distribution. It is important to note that such mechanism of laser nanostructuring has not been mentioned in previous studies, which certainly opens up prospects for further progress in the area of controlled laser writing in the volume of transparent dielectrics. We also examine the effect of refractive index nonlinearity which can lead to partial self-focusing compensating the pulse defocusing by plasma electrons.

2 MODELLING AND METHODS

Our modelling involves solving the second-order wave equation for a focused linearly polarized laser pulse moving through the fused silica in a cylindrical geometry:

$$\frac{1}{\rho}\frac{\partial}{\partial \rho}\rho\frac{\partial E}{\partial \rho} + \frac{\partial^2 E}{\partial z^2} = \frac{n^2}{c^2}\frac{\partial^2 E}{\partial t^2} + \frac{4\pi}{c^2}\frac{\partial j}{\partial t}. \quad (1)$$

In this equation, $E = E(\rho, z, t)$ denotes the electric field strength of the laser pulse as it propagates in the z-direction, n is the fused silica refractive index which includes both linear and nonlinear terms: $n = n_0 + n_2 I$. Here $n_0 = 1.45$ is the linear part of the refractive index, while the second term being proportional to laser intensity $I(\rho, z, t)$ stands for the cubic nonlinearity. According to (Vermeulen et al, 2023) we put $n_2 = 2.23 \times 10^{-16}$ cm^2/W. The second term $j(\rho, z, t)$ in right part of equation (2) is the field induced electron current. This current includes contributions from both the polarization of charge carriers within the conduction band and ionization effects caused by transitions from the valence band to

the conduction band. Both of these currents depend on the evolution of electron density $n_e(\rho, z, t)$ within the conduction band, governed by the following equation:

$$\frac{\partial n_e}{\partial t} = D\left(\frac{1}{\rho}\frac{\partial}{\partial \rho}\rho\frac{\partial n_e}{\partial \rho} + \frac{\partial^2 n_e}{\partial z^2}\right) + W_i(I)(N_0 - n_e) + v_i(I)n_e\left(1 - \frac{n_e}{N_0}\right) - \frac{n_e}{\tau_r} \quad (2)$$

Here $D \approx 300$ cm^2/s is the electron diffusion coefficient, $\tau_r = 150$ fs is the average electron recombination time (Audebert, et. al., 1990), $W_i(I)$ and $v_i(I)$ represent the rates of field-driven and electron-impact ionization, $I(\rho, z, t)$ is the laser radiation intensity, $N_0 = 2.1 \cdot 10^{22}$ см$^{-3}$ is an atomic density of fused silica. The laser intensity $I(\rho, z, t)$ is derived from the electric field as follows: $I(\rho, z, t) = \langle\frac{c}{4\pi}n_0 E^2(\rho, z, t)\rangle$, where brackets mean averaging over the period of wave field oscillations. To calculate the ionization probability we utilize the general Keldysh formula (Keldysh, 1964; Bogatskaya, et. al., 2023).

To account for the energy losses of the laser pulse due to the field ionization process, we introduce an ionization current $j_{ion}(z, t)$ on the right side of Eq. (1). This current can be expressed as

$$j_{ion}(\rho, z, t) = \frac{I_i}{\langle E \rangle}\frac{\partial n_e}{\partial t} = \frac{I_i}{\langle E \rangle}W_i(I(\rho, z, t))(N_0 - n_e(\rho, z, t)), \quad (3)$$

where $\partial n_e/\partial t$ is the rate of electron density production due to field ionization, $\langle E \rangle$ is an averaged over the period field $|E(\rho, z, t)|$. One should also consider the polarization current $j_p(\rho, z, t)$ of electrons in the conduction band, which is induced by the laser pulse. This current can be described via the Drude model:

$$\frac{\partial j_p}{\partial t} + v_{tr}j_p = \frac{e^2 n_e}{m^*}E(\rho, z, t). \quad (4)$$

Here $v_{tr} \approx 2 \times 10^{13}$ s^{-1} is the transport collisional frequency. Total current in (1) reads

$$j = j_p + j_{ion}. \quad (5)$$

The electron impact ionization is also included in the right part of equation (2). The frequency of electron impact ionization is expressed in terms [Raizer. 1977]:

$$v_i(I) = \frac{1}{I_i}\frac{4\pi e^2 I(\rho, z, t)v_{tr}}{m^* c n_0(\omega^2 + v_{tr}^2)}. \quad (6)$$

Here $m^* = 0.5m_e$ is the effective mass of charge carriers in fused silica, $\omega \approx 1.83 \times 10^{15}$ s^{-1} is the laser frequency corresponding to $\lambda_0 = 1030$ nm.

Our simulations use laser pulses with Gaussian radial profiles at the focal plane $z = 0$ ($E \sim exp(-(\rho/\rho_0)^2)$ and sin-squared temporal envelope $(E \sim E_0 sin^2\left(\frac{\pi t}{\tau_p}\right), t \in (0, \tau_p)$). To obtain such pulse, the wave equation similar to (1) but without the term of the electric current in the right-hand part was integrated with zero initial conditions for electric field strength and its derivative over time and the boundary condition at $z = 0$:

$$\left.\frac{\partial E(\rho,z,t)}{\partial z}\right|_{z=0}$$
$$= \frac{\omega n_0}{c} E_0 \exp(-(\rho/\rho_0)^2) \, sin^2\left(\frac{\pi t}{\tau_p}\right) \cos(\omega t), \quad (7)$$
$$t \in \{0^*, \tau_p\}$$

$$\frac{\partial E(\rho, z = 0, t)}{\partial z} = 0, \qquad t > \tau_p$$

The obtained pulse is considered to be the initial one in further simulations. If one reverses the time scale, this pulse will move back in negative direction towards the focal plane $z = 0$.

The focal spot radius varies from $\rho_0 = 1.7$ to 3 mkm, while the pulse duration ranges from $\tau_p = 12.5$ to 75 fs. These parameters correspond to pulse focusing within the fused silica volume with no initial free charge carriers. The spatial pulse length falls within $\ell_p = (c/n_0)\tau_p \sim 2.5 - 15$ mkm. For pulses with a 50 fs duration and focal radius $\rho_0 = 2.5$ mkm the energy range was set to 0.024 – 0.34 mkJ, yielding peak intensities of approximately $\sim 5 \times 10^{12} - 7 \times 10^{13}$ W/cm^2 at the focal plane (here we again neglect the birth of electron density in the focal plane region leading to the defocusing as a consequence, a decrease in focal intensity). For considered pulse parameters, the rate of field ionization dominates in comparison with electron impact ionization (Bogatskaya et al, 2023). Therefore, the electron avalanche, commonly seen in breakdown processes in gases and solids over microsecond and nanosecond timescales, does not control the plasma dynamics in this case. The equations (1) and (2) were solved jointly within the spatial domain $\{\rho, z\} = \{0 - \rho_0, \ 0 - L\}$ with $\rho_0 = 30$ mkm and, $L = 120$ mkm. Initial pulse ($t = 0$) was centered around $z_0 \approx 105$ μm and propagated in the negative z-direction, achieving peak focus close to the origin ($z = 30$ mkm). The numerical integration approach for the second-order wave equation is briefly described in (Bogatskaya et al, 2019).

3 RESULTS AND DISCUSSION

We start our analysis with the data on pulse focusing during the propagation in the bulk of fused silica. In Fig.1 we perform the simulations of on-axis field distributions for two values of laser peak intensity.
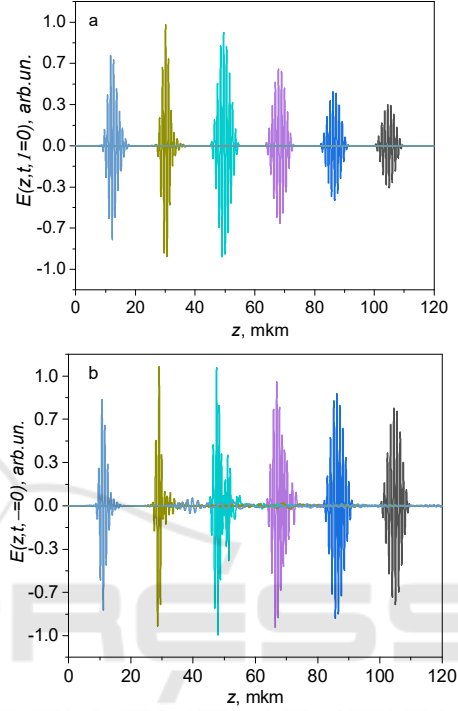

Figure 1: On-axis electric field distributions for different instants of time (intervals between time points ~ 0.1 ps). The pulse moves from right to left and focuses at point $z = 30$ mkm. Pulse peak intensity is 10^{13} W/cm^2 (a), $5 \cdot 10^{13}$ W/cm^2 (b). Focal spot radius is $\rho_0 = 2.5$ mkm, pulse duration is 50 fs.

One can see that for more intense laser pulse strong defocusing takes place due to the formation of dense plasma near the focal area. Indeed, the distributions of electron concentration for the intensity $5 \cdot 10^{13}$ W/cm^2 (see Fig.2) indicate the values of electron density more than 10^{20} cm^{-3}. In this case plasma electrons significantly defocuses and reflects laser radiation, which results in appearing rather regular structures both in the ρ- and z-axis direction. The formation of such patterns can be attributed to the coherent interference between a nearly planar incident wave in the pre-focal region and a significantly non-planar (almost spherical) wave scattered by a dense plasma burst [Bogatskaya, et al, 2024].
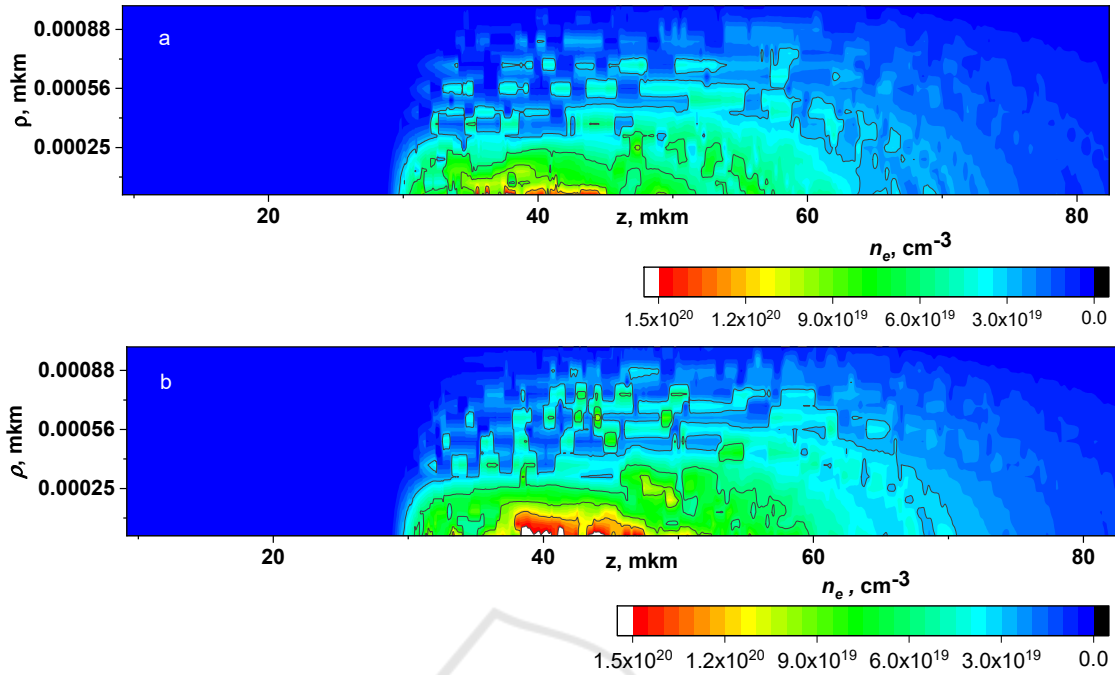
Figure 2: Profiles of electron density in the volume of fused silica formed by the 50-fs laser pulse with the peak intensity $5 \cdot 10^{13}$ W/cm2 (pulse energy is 0.24 mkJ). Graph (a) represents data in the absence of self-focusing effect, (b) – accounting the self-focusing effect. Focal spot radius is $\rho\_0 = 2.5$ mkm, the position of focal plane is 30 mkm.

In Fig.2 we also analyze the effect of refractive index nonlinearity on the plasma microstructures formation. In particular, Fig 2b presents simulations accounting n_2. Simulations have shown that in the absence of electrons the threshold of self-focusing in fused silica is about 6 MW. However, due to the strong defocusing of plasma electrons, the presence of self-focusing induced by the nonlinear refractive index has little effect on the overall picture of plasma formations. Thus, in Figure 2b one can observe that considering nonlinearity leads to a slight increase in the electron concentration in the paraxial zone near the focus.

The effect of electrons on the laser beam focusing can be clearly observed in Figure 3, which shows the dependence of the mean radius of the laser pulse during its propagation for different pulse intensities. We calculate this radius, using the following formula:

$$\langle \rho(t) \rangle = \frac{\int E^2(\rho,z,t)\rho^2 d\rho dz}{\int E^2(\rho,z,t)\rho d\rho dz}. \qquad (7)$$

At the initial instant of time the pulse is located at the point $z = 105$ mkm and moves from right to left towards the focal plane at $z = 30$ mkm. Curve 1 corresponds to the low energy pulse propagation in the absence of ionization. It can be seen that an increase of pulse energy leads to an increase in the observed beam size and a shift in the position the

focal plane (minimum value of $\langle \rho \rangle$). An increase in the focal spot size leads to a decrease in the peak intensity of the beam, as a result, ionization saturation occurs in the sample volume. This effect has been repeatedly mentioned in a number of works on focused radiation exposure in solid dielectrics (Zheltikov, 2009; Rudenko, et al, 2023).
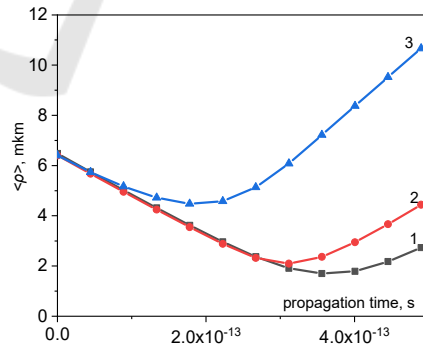

Figure 3: The radial size of the pulse $\langle \rho \rangle$ during its propagation for different pulse intensities: 1 – weak pulse, no plasma formation, 2 - 10^{13} W/cm^2, 3 - $6 \cdot 10^{13}$ W/cm^2. Plasma-free focal spot radius is $\rho_0 = 2.5$ mkm, pulse duration is 50 fs.

This study focuses on the consideration of linear polarization of the laser pulse, however, the influence of polarization on the femtosecond laser writing

process has been investigated in several experimental studies. For example, in (Lei et al, 2023) they showed that, contrary to intuitive expectations, ultrafast laser direct writing with elliptical polarization in silica glass results in birefringence approximately twice as large as that observed with linearly polarized light, although nonlinear absorption in the case of elliptical polarization is about 2.5 times weaker. Moreover, the use of laser pulses with different polarizations allows for the creation of more complex nanostructure topologies. However, the lack of theoretical studies at present complicates the possibility of controlled polarization-dependent laser writing of nanostructures.

4 CONCLUSIONS

We performed the numerical study of the effect of dense plasma formation in the volume of fused silica exposed by intense tightly focused femtosecond IR laser pulse. It was demonstrated that the plasma object with electron density at a level $\sim 1 - 2 \times 10^{20}$ cm^{-3} arises in the pre-focal plane under the conditions of tight focusing. The formed plasma effectively scatters the incident femtosecond laser pulse producing the region of effective wave interference. As a result, the spatial distribution of the electron production rate is characterized by rather sharp maxima located in the bunches of the standing wave. These maxima lead to the formation of periodic subwavelength regions of dense plasma both in ρ- and z-directions. It is important to note that the identified mechanism of volumetric self-organization is associated with a strong curvature of the front of the reflected from plasma laser wave. It was shown that due to strong beam defocusing by plasma electrons the effect of pulse self-focusing is negligible. Importantly, that the obtained profiles of plasma nanostructures are found to be in good agreement with SEM images of nanomodifications inscribed in bulk fused and crystal silica accumulation regime under the multi-pulse exposure (Zhang et al, 2019; Gulina et al, 2024). Thus, in the work (Zhang et al, 2019), the formation of periodicity in a quartz crystal was studied under the exposure of tightly focused laser pulses with wavelengths of 1030 and 800 nm at different pulse energies. The results of the experiment demonstrated the formation of extended quasi-periodic nanostructures, the spatial dimensions of which increase with increasing energy input. The similarity of the formed structures with the structures written in the volume of fused silica under the relatively equal laser focusing conditions, given in the

work of (Gulina et al, 2024), indicates the similarity of the mechanisms of the initial (plasma) stage of the nanostructuring, but later stages associated with the formation of various defects and melting zones may depend on a specific material, which requires further analysis.

In summary, the importance of understanding the process of fabrication of such periodic nanopatterns is determined by their extensive application across various fields, including optical polarizing elements and devices, light waveguides, micro-photonic crystals, binary storage components, and more (Tan et al., 2016).

ACKNOWLEDGEMENTS

REFERENCES

Audebert, P.; Daguzan, Ph.; Dos Santos, A.; Gauthier, J. C.; Geindre, J. P.; Guizard, S.; Hamoniaux, G.; Krastev, K.; Martin, P.; Petite, G.; and Antonetti, A. (1994). *Phys. Rev. Lett., 73* (14), 1990.

Beresna, M.; Gecevičius, M.; Bulgakova, N. M.; Kazansky, P. G. (2011). *Opt. Express, 19,* 18989.

Beresna, M.; Gecevičius, M.; Kazansky, P. G.; Taylor, T.; Kavokin, A. (2012). *Appl. Phys. Lett., 101,* 053120.

Bhardwaj, V. R.; Simova, E.; Rajeev, P. P.; Hnatovsky, C.; Taylor, R. S.; Rayner, D. M.; Corkum, P.B. (2006). *Phys. Rev. Lett., 96,* 057404.

Bogatskaya, A. V.; Volkova, E. A.; Popov, A. M., (2019). *Laser Phys., 29,* 086002.

Bogatskaya, A.; Gulina, Yu.; Smirnov, N.; Gritsenko, I.; Kudryashov, S.; Popov, A. (2023). *Photonics, 10,* 515.

Bogatskaya, A. V.; Volkova, E. A.; Popov, A. M., (2024). *EPL, 147* (3), 35001.

Bulgakova, N. M.; Zhukov, V. P.; Meshcheryakov, Yu. P. (2013). *Appl. Phys. B, 113(3),* 437-449.

Bulgakova, N. M.; Zhukov, V. P.; Sonina, S. V.; Meshcheryakov, Y.P. (2015). *J. Appl. Phys., 118* (23), 233108.

Dai, Y.; Patel, A.; Song, J.; Beresna, M.; and Kazansky, P. G. (2016). *Opt. Express, 24,* 19344

Desmarchelier, R.; Poumellec, B.; Brisset, F.; Mazerat, S. and Lancry, M. (2015). *World Journal of Nano Science and Engineering, 5,* 115-125.

Gattass, R. R. and Mazur, E. (2008). *Nature Photonics, 2,* 219-225.

Gulina, Yu.; Rupasov, A.; Krasin, G.; Busleev, N.; Gritsenko, I.; Bogatskaya, A.; Kudryashov, S. (2024). *JETP Lett., 119* (9), 638 – 644.

Keldysh, L.V. (1964). *JETP, 20,* 1307–1314.

Kudryashov, S. I.; Danilov, P. A.; Smaev, M. P.; Rupasov, A. E.; Zolot'ko, A. S.; Ionin A. A.; Zakoldaev, R. A. (2021). *JETP Lett., 113*, 493-497.

Kudryashov, S.; Rupasov, A.; Kosobokov, M.; Akhmatkhanov, A.; Krasin, G.; Danilov, P.; Lisjikh, B.; Abramov, A.; Greshnyakov, E.; Kuzmin, E.; et al. (2022). *Nanomaterials*, *12*, 4303.

Kudryashov, S.; Rupasov, A.; Smayev, M.; Danilov, P.; Kuzmin, E.; Mushkarina, I.; Gorevoy, A.; Bogatskaya, A.; and Zolot'ko, A. (2023) *Nanomaterials*, *13(6)*, 1133.

Lei, Y., Shayeganrad, G., Wang, H. Sakakura, M., Yu, Y., Wang, L., Kliukin, D., Skuja, L., Svirko. Y., Kazansky, P. (2023). *Light Sci Appl*, 12, 74.

Mazur, E. (2008). *Nature Photon*, *2*, 219–225.

Mermillod-Blondin, A.; Burakov, I. M.; Meshcheryakov, Y. P.; Bulgakova, N. M.; Audouard, E.; Rosenfeld, A.; Husakou, A.; Hertel, I. V.; Stoian, R. (2008). *Phys. Rev. B*, *77*, 104205.

Mizeikis, V.; Juodkazis, S.; Balciunas, T.; Misawa, H.; Kudryashov, S.I.; Ionin, A.A.; Zvorykin, V.D. (2009). *J. Appl. Phys*., *105*, 123106.

Musgraves, J.; Richardson, K.; Jain, H. (2011). *Opt. Mater. Express*, *1,* 921-935.

Raizer. Yu. P. (1977). *Laser induced discharge phenomena* (Consultants Bureau, New York)

Rudenko, A.; Moloney, J. M.; and Polynkin, P. (2023). *Phys. Rev. Applied* 20, 064035.

Schaffer, C. B.; Brodeur, A.; García, J. F.; Mazur, E. (2001). *Opt. Lett*., *26*, 93.

Shimotsuma, Y.; Kazansky, P. G.; Qiu, J. R.; Hirao, K. (2003). *Phys. Rev. Lett*., *91*, 247405.

Shimotsuma, Y.; Hirao, K.; Qiu, J. R.; Kazansky, P. G. (2005). *Modern Phys. Lett. B*, *19*, 225.

Sun, H.Y.; Song, J.; Li, C.B.; Xu, J.; Wang, X. S.; Cheng, Y.; Xu, Z. Z.; Qiu, J. R.; Jia, T. (2007) *Appl. Phys. A*, *88*, 285.

Tan, D.; Sharafudeen, K.N.; Yue, Y.; Qiu, J. (2016). *Progress in Materials Science, 76*, 154-228.

Taylor, R. S., Hnatovsky, C., Simova, E., Pattathilet, R. (2007). *Optics Letters*, *32* (19), 2888-2890.

Taylor, R.; Hnatovsky, C.; Simova, E. (2008). *Laser Photonics Rev*., *2*, 26.

Vermeulen, N.; Espinosa, D.; Ball, A. et al (2023). *J. Phys. Photonics*, 5, 035001.

Wang, Z.; Sugioka, K.; Hanada, Y.; Midorikawa, K. (2007). *Appl. Phys. A*, *88*, 699.

Zhang, F.; Nie, Z.; Huang, H.; Ma, L.; Tang, H.; Hao, M.; Qiu, J. (2019), *Opt. Express,* 27, 6442-6450.

Zheltikov. A. M. (2009). *JETP Lett*., 90, 90–95.